Optical probing of neuronal circuits with calcium indicators

Zita A. Peterlin, James Kozloski, Bu-Qing Mao, Areti Tsiola, and Rafael Yuste*

Department of Biological Sciences, Columbia University, New York, NY 10027

An experimental difficulty in unraveling circuits in the mammalian nervous system is the identification of postsynaptic targets of a given neuron. Besides ultrastructural reconstructions, simultaneous recordings from pairs of cells in brain slices have been used to identify connected neurons. We describe in this paper a technique using calcium imaging that allows rapid identification of potential postsynaptic targets. This method consists of stimulating one neuron ("trigger") while imaging a population of cells to detect which other neurons ("followers") are activated by the trigger. By using bulk-loading calcium indicators in slices of mouse visual cortex, we demonstrate that neurons that display somatic calcium transients time-locked to the spikes of a trigger neuron can be monosynaptically connected to it. This technique could be applied to reconstruct and assay circuits in the central nervous system.

An essential part of neurobiology is the characterization of circuits. Although knowledge of circuit diagrams is necessary to understand properly any computation (1), in most nervous systems the detailed circuits remain mysterious, even when the nature of the computation is clear (2). A direct approach to deciphering circuits is their reconstruction with electron microscopy. This reconstruction has been achieved only in the nervous system of *Caenorhabditis elegans*, which consists of 302 neurons with a stereotyped connectivity from animal to animal (3). For most preparations, however, electron microscopic reconstructions of entire circuits are impractical because of the high number of neurons present and the laboriousness of the serial reconstruction (4–6).

Another approach to identify circuits is to perform intracellular recordings from connected cells. This has been done extensively in invertebrate studies (7). In vertebrate preparations, dual recordings of randomly chosen neurons in brain slices have been combined with anatomical reconstructions to identify synaptic contacts (8–10). This approach, however, suffers from the problem that the probability that randomly chosen neurons are connected is low. This and the large number of neuronal classes make testing of possible connections and sequential examination of circuits impractical.

In this paper, we describe a method to identify potential postsynaptic targets of a given neuron in brain slices. We bulk-load calcium indicators into populations of neurons and then image somatic calcium transients to detect the neurons that produce action potentials (APs) time-locked to a stimulated cell. We demonstrate the usefulness of this technique by finding monosynaptically connected neurons in layer 5 from the mouse visual cortex.

Methods

Slice Preparation and Staining. Slices were made from visual cortex of postnatal day (P)12–P23 C57BL/6 mice. Animals were anesthetized with 120 mg/kg ketamine/10 mg/kg xylazine and decapitated. The brain quickly was removed and placed into cold artificial cerebrospinal fluid (ACSF; 126 mM NaCl/3 mM KCl/26 mM NaHCO$_3$/1 mM NaH$_2$PO$_4$/1 mM CaCl$_2$/3 mM MgSO$_4$/10 mM dextrose, bubbled with 95% O$_2$/5% CO$_2$). Coronal slices, 300–400 μm thick, were cut with a Vibratome

(Technical Products International, St. Louis) and were incubated at 35°C for 30 min in a submerged slice chamber. Slices were then incubated at room temperature ($\approx$25°C) for 2–12 h.

For staining, slices were transferred to a small vial with a carbogen line. We used a double-incubation protocol (11, 12): (*i*) an initial incubation with 2–5 μl of a 1 mM fura-2 acetoxymethyl ester (AM) (Molecular Probes) in 100% DMSO solution for 2 min, and (*ii*) a second incubation in 3 ml of 10 μM fura-2 AM in ACSF for 60 min. Both incubations were done in the dark. In our experience, these DMSO incubations do not have a deleterious effect on the health of the neurons, because normal resting potentials and activity from DMSO-treated slices can routinely be recorded for several hours after the procedure.

Imaging. After loading, slices were placed in a submerged recording chamber on an upright microscope (BX50WI; Olympus, New Hyde Park, NY). Experiments were done at room temperature. Fluorescent images were taken with a cooled charge-coupled device camera (Micromax; Princeton Instruments, Trenton, NJ) equipped with a frame-transfer chip (EEV 512; Kodak) or with a hexagonal photodiode array with 464 pixels (PDA; Universal Imaging, Media, PA). To maximize the number of imaged neurons, we used a 20×/0.5 numerical aperture objective (Olympus). Camera acquisition was 10–40 msec per frame, and each pixel was digitized at 12 bits. Images were acquired, stored, and analyzed with a Macintosh 7100 computer (Apple Computers) and IPLAB software (Signal Analytics, Vienna, VA). Signals from the photodiodes were amplified, sampled at 1.6 kHz, and analyzed with NEUROPLEX (Universal Imaging). For some experiments (Fig. 5), we used a silicon-intensified tube camera (C-2400; Hamamatsu, Middlesex, NJ) connected to a frame-grabbing board in a Macintosh 7600. Frames were acquired at $\approx$33 msec per frame, digitized at 8 bits, and analyzed with NIH IMAGE (National Institutes of Health).

We used a 380-nm excitation filter, a 395-nm dichroic mirror, and a 510-nm emission filter (Chroma Technology, Brattleboro, VT). We also collected images at the isosbestic excitation of 365 nm to assess the approximate intracellular Ca^{2+} concentration and therefore monitor the health of the cells. We also used the 365-nm images to estimate fura-2 concentrations, by using the fluorescence of the patched cell (with 50 μM fura-2) as a calibration, after correcting for background fluorescence and focus.

Electrophysiology. Whole-cell patch clamp recordings were performed by using 3- to 7-MΩ pipettes filled with 110–150 mM potassium gluconate or methylsulfonate/0–20 mM KCl/4–10

NEUROBIOLOGY

mM NaCl/10 mM Hepes/0–5 mM MgATP/0.05 mM fura-2 pentapotassium salt (Molecular Probes). A GΩ seal was formed in voltage-clamp and whole-cell recordings were developed with access resistances between 10 and 20 MΩ. The amplifier (Axopatch 2D; Axon Instruments, Foster City, CA) was then switched to current clamp, and the neuron was stimulated by depolarizing current steps. When necessary, current was injected to keep the resting potential at approximately −65 mV. The potential was digitized, stored, and analyzed with SUPERSCOPE (GW Instruments, Somerville, MA). Dual recordings were done with an Axopatch 200B (Axon Instruments) and a BVC-700 amplifier (Dagan Instruments, Minneapolis), and data were digitized with an analog/digital board (Instrutech, Mineola, NY) and controlled from a Macintosh 7600 running IGOR (WaveMetrics, Lake Oswego, OR).

Single-Cell Reconstruction. Neurons were filled with patch pipettes containing 1% biocytin. After fixation in 4% paraformaldehyde, slices were rinsed in PBS and incubated in 10% methanol/3% H_2O_2 for 30 min. Slices were rinsed and incubated in a horseradish peroxidase-conjugated avidin–biotin complex (Peroxidase Elite ABC Kit; Vector Laboratories) prepared in 0.75% Triton X-100 for 3 h at room temperature. Slices were then rinsed and reacted with a 2.5 mg/ml diaminobenzidine solution in Tris buffer for 20 min. Biocytin-injected neurons were revealed by the diaminobenzidine precipitate. Before final dehydration, slices were counterstained with nuclear yellow for demarcation of cortical layers.

Analysis. Changes in fluorescence were analyzed with a custom-written program. We defined the fluorescence change over time as $\Delta F/F = [(F_0 - B_0) - (F_1 - B_1)]/(F_0 - B_0)$, expressed in percent, where F_1 and B_1 are fluorescence in the somata and background fluorescence, respectively, at any given time point, and F_0 and B_0 are fluorescence in the somata and background fluorescence at the beginning of the experiment. To maximize the detection of followers, we tailored the imaging and analysis protocols to the kinetics of AP signals. Thus, with the cooled charge-coupled device camera, we used relatively slow acquisition rates (≈40 msec per frame) to image the decay phase of the calcium transient (Fig. 3). We analyzed those movies by making a $\Delta F/F$ movie and adjusting the look-up table so that the pixels recording calcium increases appeared black over a light background. This enabled the on-line (<3 min) visual detection of any imaged neuron that produced a calcium transient larger than 0.5% $\Delta F/F$. In most recordings, the signal-to-noise ratio was >3.

Results

Loading Neurons in Mature Cortical Slices with Fura 2-AM. To characterize the cortical microcircuitry present in brain slices, we sought to devise an experiment where the activity of a neuronal population could be imaged while preserving single-cell resolution in the data. In such an experiment, under ideal conditions, the stimulation of one neuron would activate its postsynaptic targets and thus reveal the cells that were connected to it. Given the complexity of the cortex, where different classes of cells presumably are carrying out specific circuit functions, we reasoned that the single-cell resolution should be an essential feature of this technique.

Voltage-sensitive dyes have been used in invertebrate preparations for reconstruction of circuit activity and connectivity (13, 14). Nevertheless, we found that their application in brain slices resulted in preferential staining of the neuropil and in small signals (15). As an alternative, we explored using calcium indicators, building on our previous work that showed that optical monitoring of the activity of neuronal populations is feasible by bulk-labeling brain slices with calcium indicators (12, 16, 17). In fact, calcium channels in the neuronal plasma
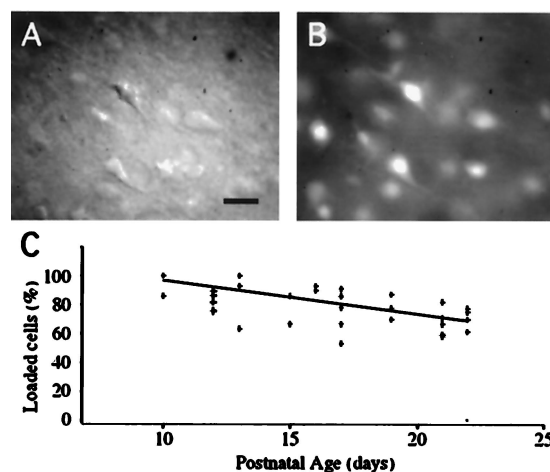
Fig. 1. Loading mature cortical slices with fura-2 AM. DIC (*A*) and fluorescence (*B*) images of the lower layers of a visual cortex slice from a P10 mouse with the pial surface to the bottom right. The slice was loaded with fura-2 AM. Somata and apical dendrites from many neurons are fluorescent, and pyramidal and nonpyramidal neurons label equally. (Scale bar = 20 μm.) (*C*) Percentage of loaded neurons as a function of the age of the animal. Each point represents one brain slice. Loading is close to 100% at P10, but it declines to ≈70% of the neurons at P20. The line represents the best linear fit.

membrane (18, 19) mediate somatic calcium transients associated with APs (17, 20). Therefore, because calcium imaging makes possible the optical detection of APs in populations of neurons (17), it should enable the identification of neurons that produce an AP in response to stimulation of another neuron.

We previously found that diluted solutions of AM forms of calcium indicators stain populations of cells in developing cortex (rats and mice <P7), but that the staining became poorer in older animals (16). We recently developed a double-incubation protocol, with concentrated DMSO solutions of fura-2 AM applied for brief periods of time, that can label a large proportion of the neurons in juvenile (P10–P30) neocortical slices (refs. 11 and 12; Fig. 1). With this protocol, we estimate that most neurons were loaded with ≈50 μM fura-2 (see *Methods*). The loading did not seem to be cell type-specific, because when differential interference contrast (DIC) images were used to classify fluorescently labeled cells, both pyramidal and nonpyramidal neurons appeared to load equally (Fig. 1 *A* and *B*). We estimated that the percentage of cells loaded with fura-2 AM ranged from ≈60% to 100%. This proportion changed from slice to slice, but followed a trend of smaller percentages of loaded cells in older animals (Fig. 1*C*).

Detecting Activation of Follower Cells After Stimulation of a Trigger Cell. After establishing that the labeling of neurons with fura-2 AM was reliable, we imaged the somata of dozens to hundreds of loaded cells during whole-cell stimulation of a particular neuron (the "trigger" cell). We carried out this work in mouse visual cortex and chose large pyramidal neurons in layer 5 as trigger cells. We included 50 μM fura-2 pentapotassium salt in the patch pipette to image the trigger.

We stimulated the trigger neuron to fire a train of APs by injecting pulses of depolarizing current (Fig. 2*A*). Each AP produced a calcium transient in the soma of the neuron with peak amplitudes of 1–5% $\Delta F/F$, time-to-peak of ≲10 msec, and decays that lasted for several seconds (Fig. 2*B*). Depolarizing pulses that did not reach threshold did not result in any detectable somatic calcium accumulations. Because the onset of the calcium transient occurred within <1 msec from the peak of the AP, by using a photodiode array with high temporal resolution
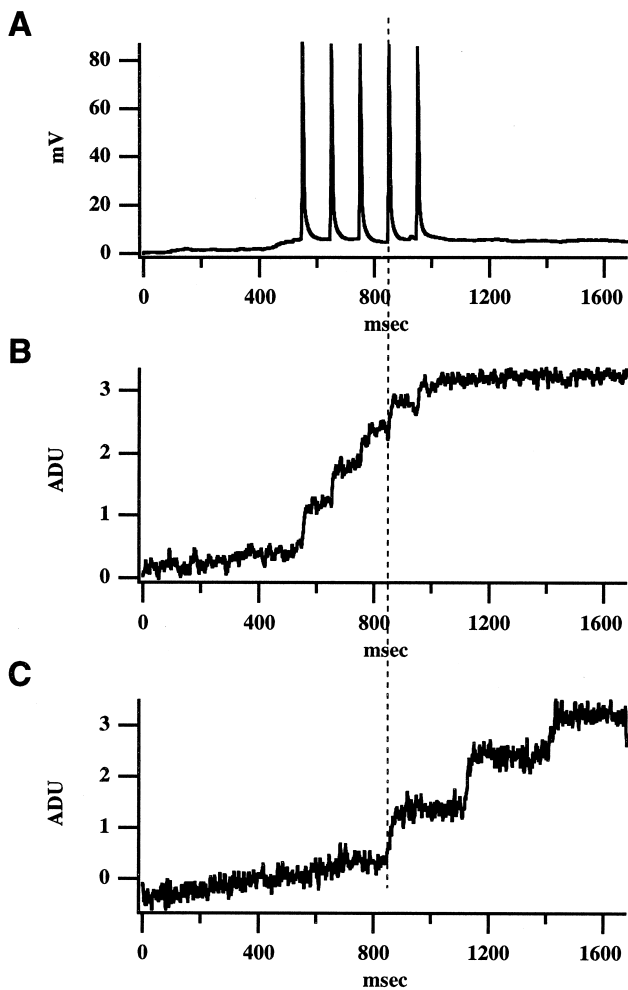
Fig. 2. Follower neuron time-locked to the stimulation of a trigger cell. (*A*) Whole-cell recording of neuron 1 (trigger). In response to five depolarizing current pulses (3 nA; 5 msec), the neuron fires five APs. (*B*) Simultaneous fluorescence measurements with a photodiode of the somatic region of neuron 1 show discrete calcium accumulations that correspond to the five APs. The sign of the fluorescence signals in all figures has been inverted. ADU, analog-digital voltage units. (*C*) Simultaneous fluorescence measurements of neuron 2 (follower), showing an intracellular calcium concentration ($[Ca^{2+}]_i$) transient phase-locked with the fourth AP of neuron 1. The onset of the calcium signal in neuron 2 occurs coincident (<0.6 msec) with the peak of the AP in neuron 1. Neuron 2 has subsequent $[Ca^{2+}]_i$ increases. The experiment was carried out in a P18 mouse cortical slice under ACSF with 2 mM Ca^{2+}/1 mM Mg^{2+}.

(0.6 msec), we could accurately follow the occurrence of each AP in the patched cell.

In our initial experiments, we found that stimulation of the trigger cell with a train of APs produced time-locked increases of the intracellular Ca^{2+} concentration in other neurons ("followers"; Fig. 2C). Because of the similarity in amplitude and kinetics of the responses in the follower cells to those elicited by a single AP in the trigger cell, we reasoned that they were also produced by single APs and that the follower neurons were brought to AP threshold by the stimulation of the trigger cell. The latency of the trigger's AP to the onset of calcium accumulation of the follower cells was, in most instances, <5 msec. Taking into account delays in axonal propagation, synaptic transmission, and time for excitatory postsynaptic potentials (EPSPs) to reach threshold, this suggested that followers were monosynaptically connected to the trigger.

Optimization of the Technique with Mg^{2+}-Free ACSF. After these results, we explored regimes where followers were easily detected. Because the light intensities necessary to measure signals with the photodiode array caused bleaching of the dye, we switched to camera imaging, at the expense of a slower temporal resolution (33 msec per frame for silicone-intensified tube analysis; 10–40 msec per frame for charge-coupled device camera). We tested different stimulation protocols. In agreement with the small size of single-axon cortical EPSPs (10, 21, 22), we never detected followers after a single AP of the trigger. Nevertheless, with trains of APs, activation of followers happened readily, suggesting that temporal summation of EPSPs was bringing the follower to threshold. To take advantage of synaptic facilitation, we used stimulations of 10 spikes at 40 Hz. Shorter trains (5 spikes), to avoid synaptic depression, did not increase the yield of the experiment. Because follower neurons were not necessarily in the same focal plane as the trigger cell, we routinely screened neurons at different focal planes.

We experimented with methods of enhancing synaptic release and of making postsynaptic cells more excitable. To decrease synaptic failures and produce larger action potential-induced calcium signals, we used 3 mM Ca^{2+} in our ACSF, which modestly increased the number of followers detected. At the same time, we noticed a marked increase in followers with Mg^{2+}-free ACSF to unblock NMDA receptors, although this manipulation increased the spontaneous activity present in the slice. In 115 trials using 2-sec imaging periods, 221 cells were active 362 times during the recording. Of those events, 108 occurred in the 840-msec period before the stimulus, 111 occurred during the 240-msec stimulation train, and 143 events occurred in the 840-msec period after the stimulus. Thus, in Mg^{2+}-free ACSF, the probability per unit time of detecting a calcium transient was increased 4.3-fold by the stimulation of the trigger cell (5.2×10^{-3} to 2.2×10^{-2} activations per cell per sec; $P < 0.0005$, Student's t test). We concluded that neurons that produced calcium transients time-locked to the stimulus were likely to be activated by the trigger cell.

Repeated Activation and Spatial Distribution of Follower Cells. The previous results suggested that, in Mg^{2+}-free ACSF, followers with time-locked responses to the trigger were probably connected to it. Nevertheless, some neurons could also produce spontaneous calcium transients time-locked to the stimulus. We reasoned, however, that spontaneous time-locked events were unlikely to occur in more than one trial. By using the probability of spontaneous activation, we estimated that the activation of an average neuron by chance during the stimulus period in two consecutive trials was 1.5×10^{-6}. Therefore, we inquired whether there were follower neurons that were activated in more than one trial and were thus likely to be connected to the trigger.

From 90 detected followers, we found that 17 cells were time-locked to the trigger in more than one trial (14/17 in consecutive trials; Fig. 3). We concluded that these neurons were probably connected to the trigger. This, however, does not imply that followers that did not repeat are not connected to the trigger cell. Interestingly, followers that were activated repeatedly were not activated in all trials (Fig. 3 *C* and *D*; see *Electrophysiological and Anatomical Confirmation of Contacts*).

We also wondered what was the laminar distribution of the followers (Fig. 3*E*). By using 380- × 380-μm fields of view centered on the trigger cell in layer 5, we detected followers in layer 5 (92%) and layer 6 (8%). The position of the followers activated more than once was similar to the total population of the followers (Fig. 3*E*, open circles). No followers were found in layer 4, although most of layer 4 and upper layer 6 were imaged in every experiment. Followers were located at distances ranging from 26 to 273 μm from the trigger (117 ± 6 μm; n = 80). We
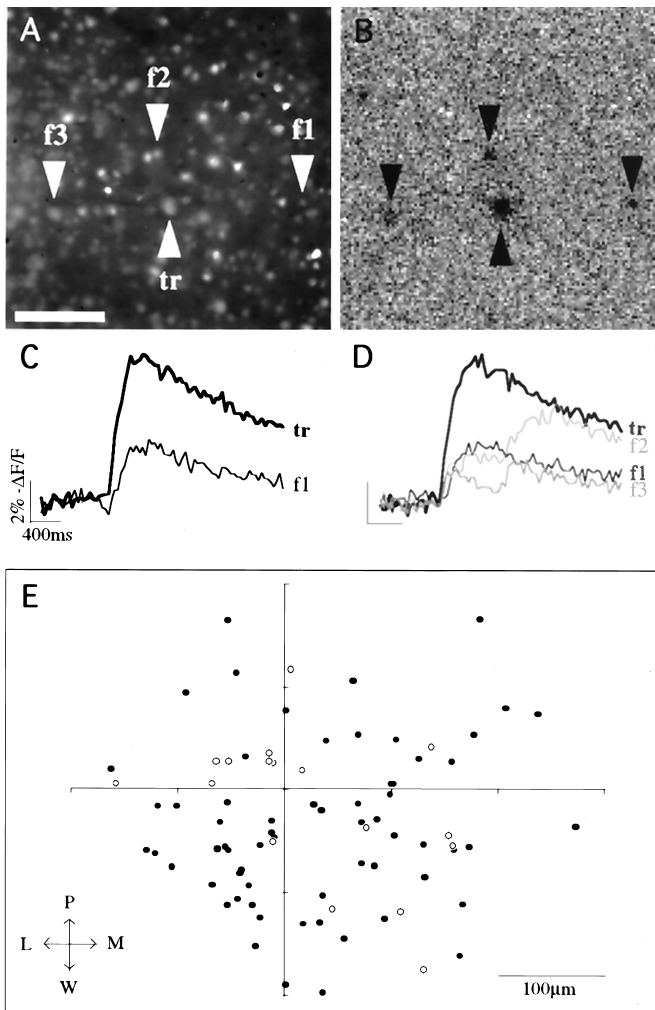
Fig. 3. Repeated activation and location of followers. (*A*) Fluorescence image of a slice from a P12 mouse showing the relative location of the trigger and three follower cells. The area imaged was a region of layer 5 with the pial surface to the upper left. The slice was maintained in Mg^{2+}-free ACSF. (*B*) Localization of followers with the processed fluorescence movie (see text). At 840 ms into the imaging, depolarizing current pulses (0.8 nA; 5 msec; 40 Hz) were used to elicit a train of 10 APs in the trigger cell. In this frame of the processed movie, corresponding to the onset of the train, four darker regions can be noted at the somata of the trigger and three follower cells. (Scale bars = 100 μm.) (*C*) Fluorescence measurements from the soma of the trigger and follower 1. The onset of the calcium signal in the follower cell occurs within 40 msec of the onset in the trigger cell. (*D*) Fluorescence measurements from the next trial with identical stimulation. Follower 1 again produces a response. In addition, two other followers have calcium accumulations during the stimulation. (*E*) Positions of followers. Center of coordinates is the position of the trigger cell. Each circle represents the somatic position of a follower cell. Open circles are followers that were activated more than once. P, pial; W, white matter; L, lateral; M, medial.

did not detect clear clustering or asymmetry of their positions, although the exact location of the chosen trigger within layer 5 changed from experiment to experiment. By using DIC, we sought to classify somatic morphologies and to inquire whether followers belonged to a specific cell class. In 15 cases in which DIC images were optimal, followers had nonpyramidal ($n = 3$) or pyramidal ($n = 12$) cell bodies.

Electrophysiological and Anatomical Confirmation of Contacts. We next inquired whether synaptic connections existed between
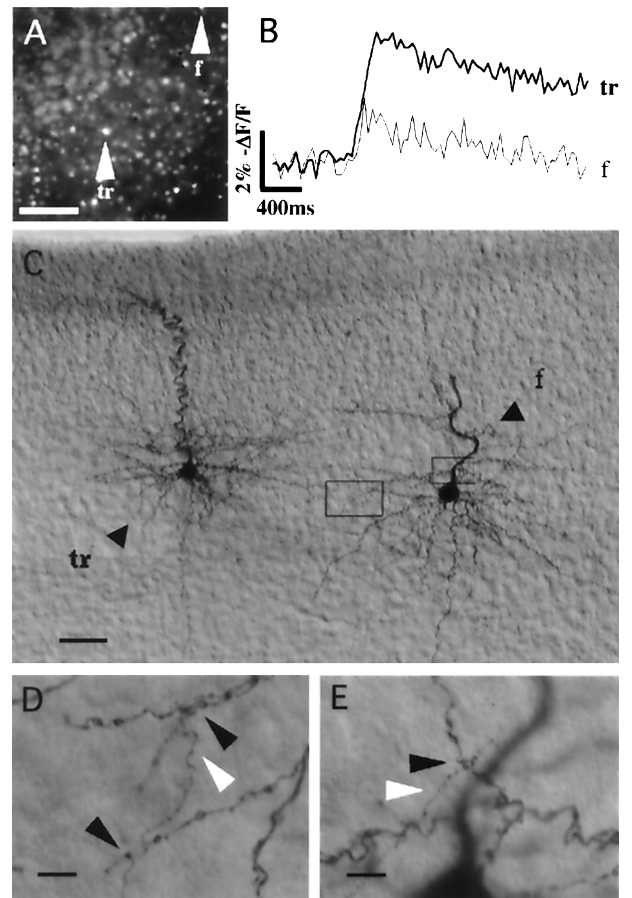
Fig. 4. Anatomical connection between trigger and follower neurons. (*A*) Fluorescence image of a slice from a P12 mouse showing the relative location of the trigger and follower cells. The area imaged was a region of layer 5 with the pial surface to the upper left. (Scale bar = 100 μm.) (*B*) Fluorescence measurements from the soma of the trigger and follower cells. (*C*) DIC photomicrograph of the two cells, after patching the follower and biocytin processing. Axonal and dendritic arbors from each cell can be distinguished. The two boxes show regions of contacts displayed in *D* and *E*. (Scale bar = 50 μm.) (*D*) Higher magnification of left box in *C*. Black arrows point at putative contacts between the axon (white arrow, vertical process) of the trigger cell and a dendrite of the follower. (*E*) Higher magnification of the right box in *C*. An additional contact can be seen. (Scale bar = 10 μm.)

trigger and follower neurons. To find anatomically synaptic contacts between the trigger and follower cells, we recorded from trigger and follower neurons with biocytin solutions and reconstructed their axonal and dendritic arbors after histological processing. In 7 of 9 reconstructions, the axon of a trigger cell seemed to physically contact the dendrite of a follower cell in at least one position (Fig. 4).

To physiologically detect connections between trigger and followers, we used dual whole-cell recordings and stimulated the trigger cell with trains of APs while recording the membrane voltage of the followers. In two experiments, one with a repeated follower and one with a follower with large optical signals, followers clearly were connected monosynaptically to the trigger, because they showed EPSPs time-locked to the APs of the trigger (Fig. 5). EPSPs summated during the train and in many, but not all, trials brought the follower cell to threshold (Fig. 5*D*). This explained the unreliable behavior of the followers described above, because the overall effect of a trigger cell is small and may not be able to consistently bring the follower neuron to threshold. These combined results indicated that the connections between trigger and follower cells can be monosynaptic.
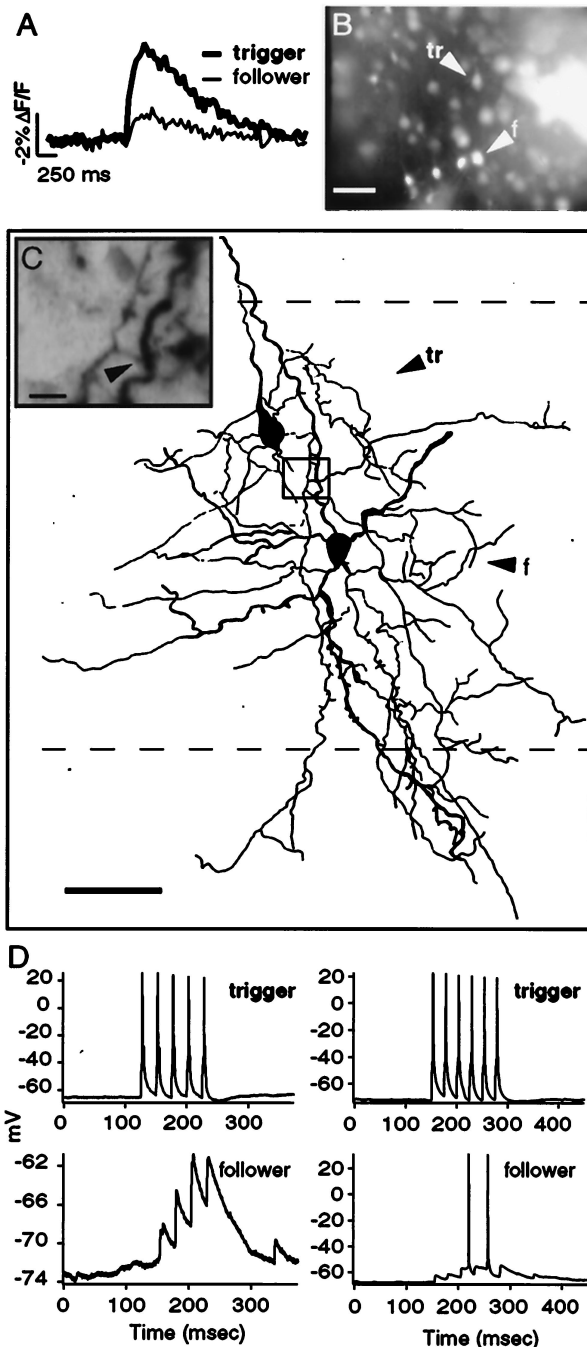
Fig. 5. Electrophysiological connection between trigger and follower neurons. (*A*) ΔF/F recordings from two neurons during single whole-cell stimulation (40 Hz; 10 pulses; 600 pA) of trigger cell. Note how trigger and follower each show clear, time-locked fluorescence changes in response to APs evoked in trigger cell. (*B*) A second whole-cell patch recording from the optically identified follower is established. (Scale bar = 50 μm.) Note bulk-loading of fluorescent calcium indicators in neighboring cells. (*C*) Camera lucida reconstruction of biocytin labeling reveals both cells' morphology, and a region of overlap between trigger cell axons and follower dendrites. Lines represent borders of layers 4/5 and 5/6. (Scale bar = 50 μm.) (*Inset*) Potential contacts between trigger axon and follower dendrite. (Scale bar = 20 μm.) (*D*) Paired recordings from trigger and follower. During stimulation of trigger, EPSPs were clearly visible in the follower neuron. Follower EPSPs initiated with a 1.25–2.1 msec latency to the peak of the trigger cell's APs (*Left*) and showed temporal summation. Note that failures of EPSPs were observed (*Left*, first trigger spike), and that spiking could be evoked in the follower cell, but unreliably (*Right*).

Discussion

In this paper, we present the implementation of a simple idea to detect the excitation of target neurons (followers) from any given neuron (trigger) by using calcium imaging of populations of neurons in brain slices. We show five different lines of evidence indicating that the trigger and follower cells can be monosynaptically connected. First, the onset of the response of the follower can occur within 1 msec of the peak of an AP of the trigger (Fig. 2). Second, in Mg^{2+}-free ACSF, followers occur time-locked to the stimulus trains at probabilities that are statistically different from spontaneous activation. Third, followers can be activated in more than one trial (Fig. 3). Fourth, the axon of the trigger can be traced to the dendrites of the follower, and contacts are found at the light microscopy level (Fig. 4). Fifth, followers can receive EPSPs from trigger cells (Fig. 5). Taken together, our data suggest that trigger cells can form axodendritic monosynaptic contacts with follower cells.

Nevertheless, alternative scenarios can also explain some of our results. Followers could be activated polysynaptically by the trigger. We imagine that the small size of cortical EPSPs would make polysynaptic activation caused by a single trigger extremely unlikely, because the effect of any excitatory cortical neuron on another cell is small (refs. 10, 21, and 22; Fig. 5). At the same time, we have detected followers with activation hundreds of milliseconds after the end of the train of APs in the trigger cell (Figs. 2 and 3). It is possible that in those cases, the follower remained close to threshold and was brought to spike by background EPSPs. Also, some followers may be spontaneously active during the stimulus train.

Which followers are connected to the trigger? The answer to this crucial question depends on the experimental conditions, because the temporal resolution of the imaging and the ACSF composition influence the probability of occurrence of spontaneous events time-locked to the stimulation and, therefore, of detecting connected followers. Although, based on the anatomical reconstructions, we believe that under our experimental conditions most followers are probably connected to the trigger, short of performing dual whole-cell recordings with each trigger–follower pair, this cannot be argued unambiguously. However, it seems to us that if a follower becomes activated in two different trials, it is very likely be connected to the trigger, because of the low probability of this event happening by chance. Indeed, by using this criterion, we selected a follower whose connection was later confirmed with dual whole-cell recording (Fig. 5).

Advantages of Optical Probing. A benefit of this optical probing technique is the quick identification of candidate targets of a given neuron. As we demonstrate (Fig. 5), it can be used to select neurons for dual recording experiments. This will enable investigators to detect and study connected targets, regardless of the proportion of the target in the circuit. Optical probing can also help in finding targets at a distance from the stimulated cell, in finding sequential targets, or in other situations where recording from randomly chosen cells is impractical.

In addition, in experiments where the selection of connected followers is properly calibrated, this technique can obviate the need to record from the postsynaptic neuron to identify whether a connection exists. In this manner, this technique could be used to rapidly reconstruct circuits or to assay the functional state of a particular connection or a circuit, enabling the examination of the effect of neuromodulators or pharmacological agents.

A consequence of this technique is that stronger connections are revealed at the expense of weaker ones. Because this method requires postsynaptic suprathreshold depolarization, connections made with multiple contacts or with synapses of higher efficacy will be the first ones detected. This bias may be an

NEUROBIOLOGY

advantage in areas with distributed connections, because it will select for connections that are more effective in driving the circuit.

Another advantage of this technique is that the strength and reliability of individual synaptic connections can be tested in parallel. Thus, studies can be done simultaneously in multiple postsynaptic neurons, stimulating the trigger with protocols to induce potentiation or depression in target cells, or to examine whether particular temporal patterns of activity excite specific types of followers.

A final advantage of this technique is that it does not require complex equipment. As we show in Fig. 5, because of the large amplitude of the optical signals, APs can be detected in neuronal populations with silicon-intensified tube cameras and 8-bit digitization boards.

Modifications of the Technique and Future Directions. One limitation of this approach is that it only reveals excitatory connections. Nevertheless, it could be used under high-background spontaneous activity, induced pharmacologically as described above. In this case, stimulation of an inhibitory trigger could produce a time-locked inhibition of the APs of followers. Also, Cl⁻ indi-

cators could enable direct imaging of inhibitory connections (23). A second limitation with this approach is that it reveals only suprathreshold targets, although the excitability of the slice can easily be manipulated to turn initially subthreshold events into suprathreshold ones and to reveal a larger selection of targets.

An exciting prospect of this technique is its use with genetically encodable activity-sensitive indicators, like calmodulin–green fluorescent protein indicators (24, 25) or potassium-channel green fluorescent protein constructs (26). Besides possible improvements in signal-to-noise ratio and possible measurements of EPSPs, genetic indicators could be expressed specifically, enabling the piecemeal analysis of circuits. Also, animals expressing these indicators in cortical neurons could enable *in vivo* experiments with two-photon microscopy (27) and could allow detection of long-distance targets. In an ideal case, optical probing could also be combined with computerized photostimulation (28, 29) of individual trigger neurons to make possible a fast and systematic reconstruction of circuits.

1. Marr, D. (1982) *Vision* (Freeman, New York), pp. 23–27.
2. Heiligenberg, W. (1991) *Neural Nets in Electric Fish* (MIT Press, Cambridge, MA).
3. White, J. G., Southgate, E., Thomson, J. N. & Brenner, S. (1986) *Philos. Trans. R. Soc. London B* **314,** 1–340.
4. Freund, T. F., Martin, K. A., Somogyi, P. & Whitteridge, D. (1985) *J. Comp. Neurol.* **242,** 275–291.
5. McGuire, B. A., Gilbert, C. D., Rivlin, P. K. & Wiesel, T. N. (1991) *J. Comp. Neurol.* **305,** 370–392.
6. Czeiger, D. & White, E. L. (1993) *J. Comp. Neurol.* **330,** 502–513.
7. Marder, E. & Calabrese, R. L. (1996) *Physiol. Rev.* **76,** 687–717.
8. Gulyas, A. I., Miles, R., Sik, A., Toth, K., Tamamaki, N. & Freund, T. F. (1993) *Nature (London)* **366,** 683–687.
9. Buhl, E. H., Halasy, K. & Somogyi, P. (1994) *Nature (London)* **368,** 823–828.
10. Deuchars, J., West, D. C. & Thomson, A. (1994) *J. Physiol.* **478,** 423–435.
11. Schwartz, T., Rabinowitz, D., Unni, V. K., Kumar, V. S., Smetters, D. K., Tsiola, A. & Yuste, R. (1998) *Neuron* **20,** 1271–1283.
12. Yuste, R. (1999) in *Imaging Neurons: A Laboratory Manual*, eds. Yuste, R., Lanni, F. & Konnerth, A. (Cold Spring Harbor Lab. Press, Plainview, NY), 34.1–34.9.
13. Cohen, L. B. & Lesher, S. (1986) in *Optical Methods in Cell Physiology*, eds. De Weer, P. & Salzberg, B. M. (Wiley Interscience, New York), pp. 72–99.
14. Cacciatore, T. W., Brodfuehrer, P. D., Gonzalez, J. E., Jiang, T., Adams, S. R., Tsien, R. Y., Kristan, W. B. & Kleinfeld, D. (1999) *Neuron* **23,** 449–459.
15. Yuste, R., Tank, D. W. & Kleinfeld, D. (1997) *Cereb. Cortex* **7,** 546–558.
16. Yuste, R. & Katz, L. C. (1991) *Neuron* **6,** 333–344.
17. Smetters, D., Majewska, A. & Yuste, R (1999) *Methods* **18,** 215–221.
18. Yuste, R., Gutnick, M. J., Saar, D., Delaney, K. D. & Tank, D. W. (1994) *Neuron* **13,** 23–43.
19. Johnston, D., Magee, J. C., Colbert, C. M. & Christie, B. R. (1996) *Annu. Rev. Neurosci.* **19,** 165–186.
20. Helmchen, F., Imoto, K. & Sakmann, B. (1996) *Biophys. J.* **70,** 1069–1081. R. Y.
21. Mason, A., Nicoll, A. & Stratford, K. (1991) *J. Neurosci.* **11,** 72–84.
22. Markram, H. & Tsodyks, M. (1996) *Nature (London)* **382,** 807–810.
23. Inglefield, J. R. & Schwartz-Bloom, R. D. (1999) *Methods* **18,** 197–203.
24. Romoser, V. A., Hinkle, P. M. & Persechini, A. (1997) *J. Biol. Chem.* **272,** 13270–13274.
25. Miyawaki, A., Llopis, J., Heim, R., McCaffery, J. M., Adams, J. A., Ikura, M. & Tsien, R. Y. (1997) *Nature (London)* **388,** 882–887.
26. Siegel, M. S. & Isacoff, E. Y. (1997) *Neuron* **19,** 735–741.
27. Denk, W., Delaney, K. R., Gelperin, A., Kleinfeld, D., Strowbridge, B. W., Tank, D. W. & Yuste, R. (1994) *J. Neurosci. Methods* **54,** 151–162.
28. Farber, I. C. & Grinvald, A. (1983) *Science* **222,** 1025–1027.
29. Callaway, E. M. & Katz, L. C. (1993) *Proc. Natl. Acad. Sci. USA* **90,** 7661–7665.